

BIOCHEMISTRY

Conditional iron and pH-dependent activity of a non-enzymatic glycolysis and pentose phosphate pathway

Markus A. Keller,^{1*†} Andre Zylstra,¹ Cecilia Castro,¹ Alexandra V. Turchyn,² Julian L. Griffin,^{1,3} Markus Ralser^{1,4†}

2016 © The Authors, some rights reserved; exclusive licensee American Association for the Advancement of Science. Distributed under a Creative Commons Attribution NonCommercial License 4.0 (CC BY-NC). 10.1126/sciadv.1501235

Little is known about the evolutionary origins of metabolism. However, key biochemical reactions of glycolysis and the pentose phosphate pathway (PPP), ancient metabolic pathways central to the metabolic network, have non-enzymatic pendants that occur in a prebiotically plausible reaction milieu reconstituted to contain Archean sediment metal components. These non-enzymatic reactions could have given rise to the origin of glycolysis and the PPP during early evolution. Using nuclear magnetic resonance spectroscopy and high-content metabolomics that allowed us to measure several thousand reaction mixtures, we experimentally address the chemical logic of a metabolism-like network constituted from these non-enzymatic reactions. Fe(II), the dominant transition metal component of Archean oceanic sediments, has binding affinity toward metabolic sugar phosphates and drives metabolism-like reactivity acting as both catalyst and cosubstrate. Iron and pH dependencies determine a metabolism-like network topology and mediate reaction rates over several orders of magnitude so that the network adopts conditional activity. Alkaline pH triggered the activity of the non-enzymatic PPP pendant, whereas gentle acidic or neutral conditions favored non-enzymatic glycolytic reactions. Fe(II)-sensitive glycolytic and PPP-like reactions thus form a chemical network mimicking structural features of extant carbon metabolism, including topology, pH dependency, and conditional reactivity. Chemical networks that obtain structure and catalysis on the basis of transition metals found in Archean sediments are hence plausible direct precursors of cellular metabolic networks.

INTRODUCTION

The origin of metabolism was one of the crucial early evolutionary developments and rendered the first organisms independent of obtaining biochemical constituents such as carbohydrates (1, 2), amino acids (3), or nucleobase precursors (4, 5) and their possible phosphorylation (6) from the environment. Before enzymes were in place, the first biomolecules must have formed by chemical means, achieving a non-enzymatic chemistry that allowed the first organisms to establish compartments and rudimentary genetic mechanisms (4, 7–10). However, little is known how life then managed to switch away from using non-enzymatic reactions by establishing a metabolic network. A key question concentrates around the problem of whether the conserved metabolic network structure in modern organisms is a result of genetics or descends from a preserved non-enzymatic core (11, 12). A major restriction towards the formed molecules is that Darwinian evolution can only select for a functional product, rather than for an intermediate, and dictates that metabolic pathways originate as functional systems (9, 10). A likely scenario for the origin of first metabolic pathways hence involves non-enzymatic reaction sequences that form a template on which a stepwise selection of early enzymes or ribozymes can commence (13). The large compendium of entries in the Beilstein database of molecules and reactions are indicative of an enormous chemical space, which is contrasted by the (comparatively) small proportions of reactions that participate in

the metabolic network. The key for shaping the modern metabolic network could hence indeed be the dependency on a restricted number of inorganic catalysts, which would have reduced the chemical space to those reactions achievable with the simple molecules available (14–16). However, a limitation to this interpretation has been that enzymes use highly complex structures to achieve metabolic reactivity, creating skepticism that a critical set of metabolism-like reactions is indeed achievable with environmentally available inorganic catalysts (17, 18). Such scenario, however, has recently gained plausibility after the discovery of a series of non-enzymatic and mutually compatible pendants for metabolic reactions that constitute the (partially overlapping) metabolic pathways glycolysis, gluconeogenesis, and pentose phosphate pathway (PPP) in the modern cell (19). Although these pathways exist in several variations, such as the Embden-Meyerhof-Parnas and Entner-Doudoroff pathways, most of the interconversions depend on the same reactions and play a virtually universal role in providing precursors for the synthesis of nucleotides, amino acids, lipids, and energy cosubstrates, implying an origin of these pathways at an early stage of evolution (20–24).

Here, we address the chemical properties of a network of non-enzymatic glycolytic and PPP-like reactions. We found these to be largely sensitive to Fe(II) participating as a cosubstrate and/or catalyst. A non-enzymatic chemical network assembled from these reactions is strongly influenced by pH, causing reaction rates to vary over several orders of magnitude. Systematic quantification of the time/iron/pH dependency landscapes for 26 metabolism-like non-enzymatic reactions in more than 4000 liquid chromatography–tandem mass spectrometry (LC-MS/MS) experiments reveals that similar reactivity and iron/pH profiles distinguish non-enzymatic glycolytic from non-enzymatic PPP reactions. Moderate changes in pH thus affect network dynamics and the distribution of reactivity within the two non-enzymatic pathways that resemble central carbon metabolism in the enzymatic world.

¹Department of Biochemistry and Cambridge Systems Biology Centre, University of Cambridge, 80 Tennis Court Road, Cambridge CB2 1GA, UK. ²Department of Earth Sciences, University of Cambridge, Downing Street, Cambridge CB2 3EQ, UK. ³MRC Human Nutrition Research, Elsie Widdowson Laboratory, 120 Fulbourn Road, Cambridge CB1 9NL, UK. ⁴The Francis Crick Institute, Mill Hill Laboratory, The Ridgeway, Mill Hill, London NW7 1AA, UK. *Present address: Division of Biological Chemistry, Biocenter, Medical University of Innsbruck, 6020 Innsbruck, Austria. †Corresponding author. E-mail: mk747@cam.ac.uk (M.A.K.); mr559@cam.ac.uk (M.R.)

RESULTS

The interaction of metabolic sugar phosphates with iron in aqueous solution

Non-enzymatic glycolytic and PPP-like reactions are sensitive to the presence of metal ions, particularly iron (19). We speculated that, to achieve metabolism-like reactions, metal ions have to directly interact with the metabolites. Fe(II) is a highly concentrated metal in Archean oceanic sediments (25, 26) and was the strongest single contributor to specific sugar phosphate interconversions (19). ^1H nuclear magnetic resonance (NMR) spectroscopy was used to investigate its ability to bind R5P and 6PG, metabolites that are part of the PPP and that react non-enzymatically in a PPP-like manner (19), by exploiting the paramagnetic properties of $\text{Fe}^{2+}/\text{Fe}^{3+}$ ions; their unpaired electrons alter

the NMR properties of surrounding solvated molecules (27). Specifically, the three main effects that can be observed upon metal-ligand interactions are changes in chemical shift and shortening of the spin-lattice relaxation times (T_1) and spin-spin relaxation times (T_2) (28, 29).

Exposing 20 mM R5P to Fe(II) and Fe(III) at increasing concentrations revealed an interaction of the sugar phosphate with Fe(II), shown by the shortening of the T_2 relaxation times and changes in chemical shifts (Fig. 1A, left panel, and fig. S1). Asymmetric changes of signal intensities allowed to identify the strongest response within protons closest to the phosphate group (positions 5 and 10 at 3.85/3.91 ppm), implying that the positively charged metal ion binds primarily to the negatively charged phosphate group. Furthermore, Fe(II) triggered conformational changes within the R5P molecule, as revealed by the T_1 relaxation time experiments (table S1): Fe(II) initiates a rapid initial drop

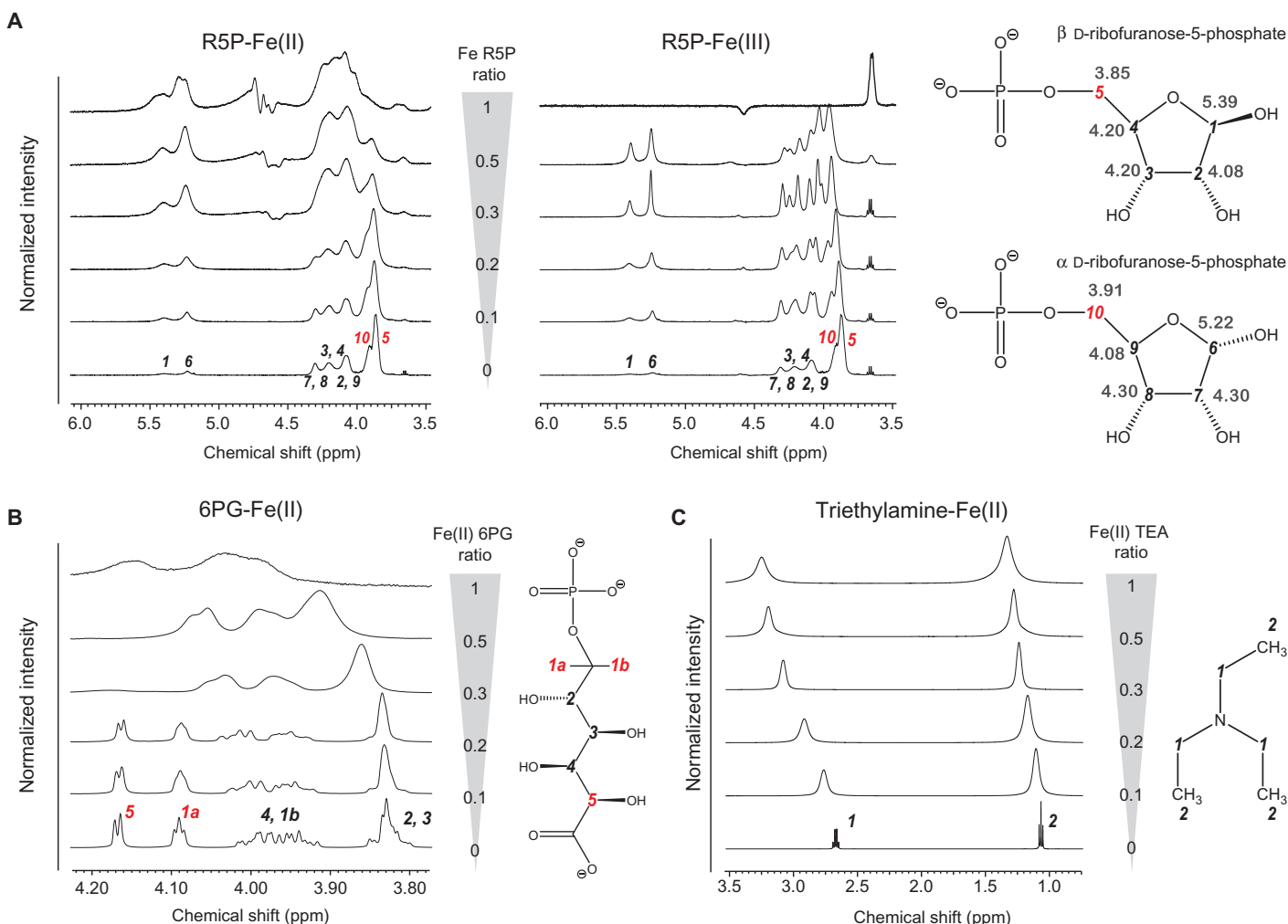


Fig. 1. Metabolite/iron interactions are facilitated by negative charge and phosphate residues. (A) Fe(II) (left panel) or Fe(III) (central panel) was combined up to equimolar levels with 20 mM ribose-5-phosphate (R5P). ^1H NMR spectra were recorded to monitor peak broadening (T_2) induced by iron proximity. Fe(II) spectra reveal an asymmetric effect on the molecule (that is, compare peaks 5 and 10 with 2, 4, and 9). Right panel: Peak assignment to the ^1H NMR signals with protons next to negatively charged groups (highlighted in red). For optimal peak visualization, spectra are normalized to the respective maximum peak (table S5 for integrated peak areas). Iron binding suppresses R5P signals with increasing concentrations. (B) Similar to (A) but with 6-phosphogluconate (6PG) and Fe(II). Peaks 1 and 5, which are closest to the carboxyl and phosphoryl groups, are the most affected by iron and indicate initial binding at these sites (table S5 for integrated peak areas). (C) Similar to (A) but with triethanolamine and Fe(II) as control. Here, no comparable Fe(II) effect is observed (table S5 for integrated peak areas). For all experiments, one of three representative replicates is shown. Complete iron dilution series and T_1 experiment results are given in figs. S1 to S4 and tables S1 to S4.

in the average distance (corresponding to T_1) between the metal and the section of R5P in proximity to the phosphate group [3.85, 3.91, and 5.39 ppm at 0.2 μM Fe(II)], whereas, at higher Fe(II) concentrations, this was partially reversed, indicating structural rearrangements. At equimolar Fe(II) concentration, the T_1 for most protons was too short to be reliably measured. Together, this shows that Fe(II) interacts differently with the $\alpha\text{-D}$ and $\beta\text{-D}$ forms of ribofuranose-5-phosphate (Fig. 1A), which was not observed to the same extent for Fe(III), that was following a much more linear behavior (Fig. 1A, fig. S2, and table S2).

The carboxyl group of 6PG represents another anionic group that did facilitate additional iron binding reflected in the T_1 and ^1H NMR data, which indicates close proximity of protons near the 6PG phosphate and carboxyl groups [nuclei (1) and (5); Fig. 1B, fig. S3, and table S3]. As control, we performed a similar study using cationic triethylamine as substrate (Fig. 1C) and observed general T_2 -related peak broadening, common to all proton groups in the triethylamine molecule, without comparable disruption of peak integrity (fig. S4 and table S4).

Fe(II) functions as cosubstrate in 6PG and R5P metabolism-like reactivity

Iron-dependent sugar phosphate reactivity was studied in 5-hour time course experiments, conducted at 70°C in an anoxic chamber by quantifying obtained samples via *n*-octylammonium acetate-enhanced LC-MS/MS analysis (19, 30). Different roles of iron on sugar phosphate reactivity were revealed, as exemplified for three representative metabolism-like reactions: resembling the PPP, 6PG is non-enzymatically converted into R5P exclusively in the presence of iron, with fast initial product formation within 60 min, followed by subsequently decreasing R5P levels (Fig. 2B, top). In contrast, the isomerization rate of R5P into xylulose-5-phosphate and ribulose-5-phosphate (X5P/Ru5P), occurring downstream in the PPP, was decreased in the presence of iron and reached a steady state after 2 hours (Fig. 2B, central). A third type of profile is exemplified by the non-enzymatic pendant of the glycolytic interconversion of phosphoenolpyruvate to pyruvate (PEP→Pyr). This occurred slowly without metal but was strongly accelerated by iron (Fig. 2B, bottom). All three reactions were hence influenced by Fe(II), although in a different manner.

Fe(II) oxidation triggers the formation of Fe(OH)₃ complexes that withdraw hydroxide ions, which would result in acidification. In the absence of metabolites, 90% of iron remained detectable as Fe(II) over the 5-hour time course (Fig. 2C, full line), whereas 10% formed insoluble Fe(OH)₃ complexes (Fig. 2, D, red full lines, and E, full line). In the presence of 6PG and R5P, Fe(II) concentration decreased faster (Fig. 2C, dotted lines) and triggered a drop in pH, from between 6.1 and 6.5 to 4.9 (Fig. 2D, red dotted lines). Here, Fe(OH)₃ formation only explained 55 to 70% of Fe(II) depletion (Fig. 2E). In agreement with literature, this finding implied the formation of various Fe(II)/Fe(III) complexes with organic compounds, water, and/or hydroxyl ions in a pH- and concentration-dependent manner (31). We confirmed this pH-dependent iron complex formation by ultraviolet-visible (UV-vis) spectroscopy (Fig. 2F), showing that, at low pH, ferrous Fe(II) complexes were stabilized, whereas at higher pH, the balance shifted toward ferric ions (fig. S6). Sugar phosphate-iron profiles are distinct from the isolated molecules, indicating pH-dependent complex formation (Fig. 2F). Despite significantly accelerating the third reaction, Fe(II) levels remained largely unaffected by the presence of the PEP (Fig. 2C, dashed line). Here, the solution is already initially acidified and stabilized Fe(II) (Fig. 2D).

Strong pH dependencies dominate non-enzymatic reactions

We continued by determining pH dependencies for the whole spectrum of non-enzymatic metabolism-like reactions that start from glycolytic and PPP intermediates. Phosphate was considered a suitable buffer system because its existence in Archean aqueous environments is suggested by the geological record. Additionally, the presence of phosphate in early life forms is indirectly confirmed by it being a part of many essential molecules, including the RNA backbone (17). Finally, compared to other inorganic buffer systems, the three possible dissociations of phosphoric acid ($\text{p}K_{\text{a}1} = 2.148$, $\text{p}K_{\text{a}2} = 7.498$, and $\text{p}K_{\text{a}3} = 12.319$) allow a broader spectrum of accessible pH values. The phosphate buffer was used at a 25-fold concentration compared to iron (200 μM) to minimize pH fluctuations induced by the reactions themselves. Thirteen metabolites were in triplicate exposed to seven pH conditions and continuously sampled over 5 hours. Experiments were conducted in the presence and absence of Fe(II), at a concentration considered a realistic average for an Archean ocean environment according to sediment constitutions (32). Samples were analyzed in more than 4000 LC-MS/MS runs that yielded quantities for 26 metabolism-like non-enzymatic reactions. An illustrative example is a reaction sequence starting from 6PG that resembles the PPP. 6PG reacted to R5P (Fig. 3A, top left panel) fastest at an acidic pH, whereas 6PG to E4P accelerated at neutral/basic pH (Fig. 3A, top central panel). Studying individual intermediates explained the bimodality: R5P is formed as an initial product and further reacts into E4P at pH >7, and R5P is thus only accumulating at pH <6 (Fig. 3A, top right panel).

In contrast, the isomerization of R5P to X5P/Ru5P is slightly faster without Fe(II) (Fig. 3A, bottom left panel), potentially explained by the formation of E4P and Pyr at neutral/basic pH (Fig. 3A, bottom left and central panels). The PEP-to-Pyr reaction was instead fastest at acidic pH (Fig. 3A, bottom right panel). Here, the rate between the Fe(II) and Fe(II)-free solutions was indifferent. This indicated that, in contrast to other reactions, this reaction had been solely affected by pH.

We observed no pentose formation from G6P, whereas such reactivity was found for the isomer F6P. A possible explanation is that F6P prefers a furanose ring conformation facilitating C-C bond breakage required to yield X5P/Ru5P and R5P, whereas G6P is predominantly present as a six-membered pyranose ring (33). This notion is consistent with the 2.5-fold and significantly lower reactivity of G6P ($P = 0.0063$, $n = 6$; pH 8 to 9) under alkaline conditions, contrasting with F6P that reacts faster at alkaline pH (Fig. 4A), whereas at acidic pH ($P = 0.94$, $n = 6$; pH 3 to 5), where pentose sugar phosphate production from G6P and F6P is inactive, their total reactivity is similar.

Strong pH dependency within a non-enzymatic glycolysis and PPP

In total, for 19 of the 26 reactions, we detected significant pH dependency (Welch's unequal variances *t* test, $P < 0.05$) by more than twofold. In 17 cases, the fastest-to-slowest rate differed by more than one order of magnitude (Fig. 3B and tables S6 to S9), and in 4 cases, pH changes could completely abolish reactivity (Fig. 3B, bottom left). pH dependency was also observed for 15 iron-independent reactions, of which 12 were accelerated by more than one order of magnitude (Fig. 3B). In total, only eight reactions were slower in the presence of Fe(II) so that reactivity within the total system, expressed as median, was accelerated 3.15-fold in the presence of Fe(II). The total decomposition

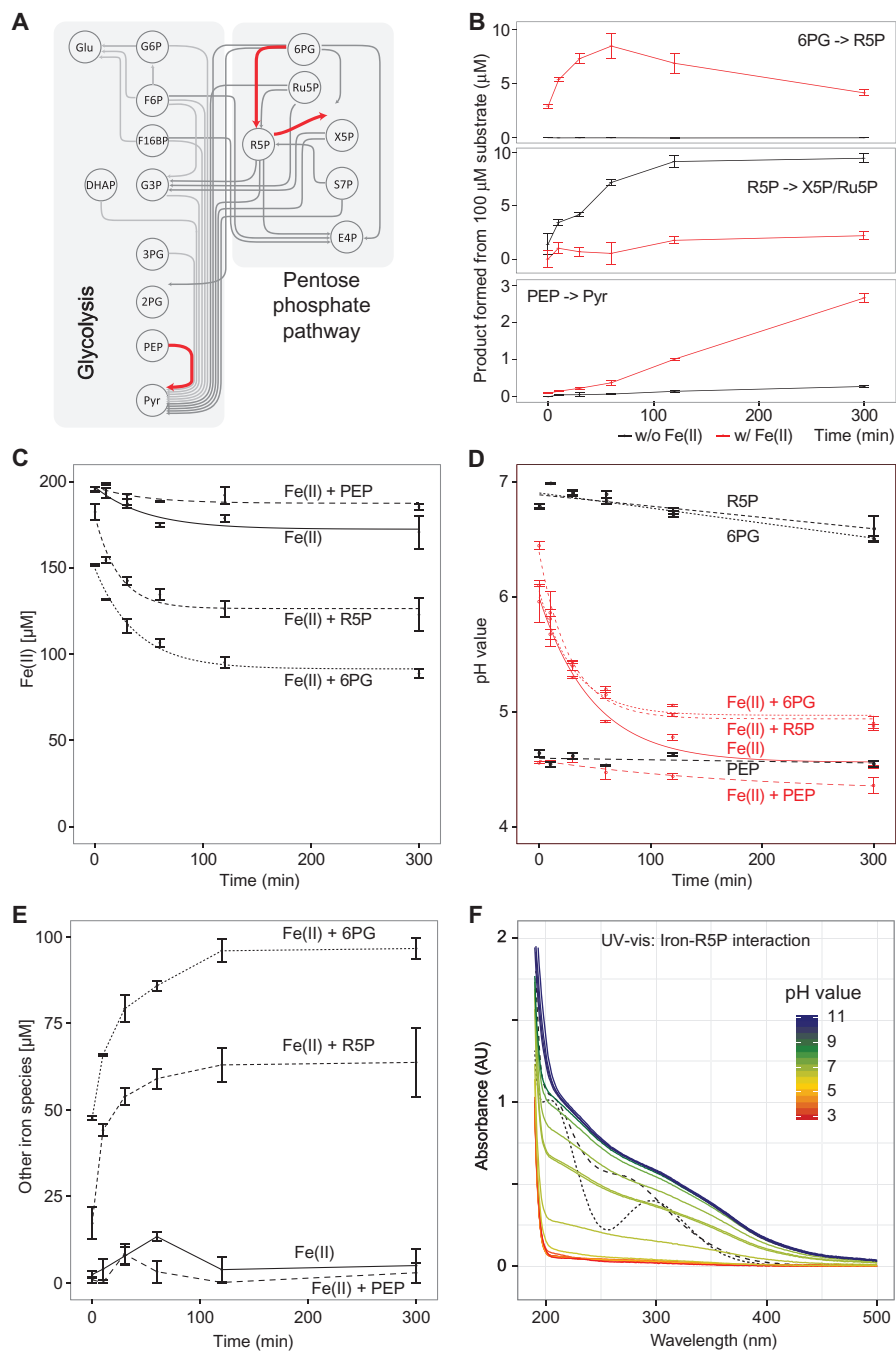


Fig. 2. The role of iron in metabolism-like interconversions among sugar phosphates. (A to F) Under anoxic conditions and in the presence of Fe(II), non-enzymatic reactivity interconverts glycolytic and PPP metabolites (A). Illustrated is a network graph from the panel of non-enzymatic reactions detected in the presence of Archean sediment metals (19), reflecting topological features of glycolysis and the PPP (the illustration orients the Embden-Meyerhof pathway). The exemplary reactions used in (B) to (F) are highlighted in red. DHAP, dihydroxyacetone phosphate; G6P, glucose 6-phosphate; F6P, fructose 6-phosphate; F16BP, fructose 1,6-bisphosphate; G3P, glyceraldehyde 3-phosphate; 3PG, 3-phosphoglyceric acid; S7P, sedoheptulose 7-phosphate; E4P, erythrose-4-phosphate. (B) Representative examples of metabolism-like non-enzymatic sugar phosphate interconversions. LC-selective reaction monitoring (LC-SRM) absolute quantification was used to measure the time-dependent formation of R5P from 6PG (upper panel), X5P/Ru5P from R5P (center panel), and Pyr from PEP (lower panel) quantified in the presence (red lines) and absence (black lines) of 200 μM Fe(II) in aqueous, anoxic solution. Data are expressed as means \pm SD ($n = 3$). (C) Availability of Fe(II) in (B) over time. Fe(II) (200 μM) without substrate added was included as control; data are expressed as means \pm SD ($n = 3$). (D) pH changes during the reactions as in (C) in the presence (red) or absence (black) of iron. Data are expressed as means \pm SD ($n = 3$). (E) Formation of iron species other than free Fe(II) and Fe(III) contained in hydroxy complexes. Data are expressed as means \pm SD ($n = 3$). (F) UV-vis absorption spectra of 100 μM R5P and 200 μM Fe(II) at different pH. pH was adjusted with HCl and KOH, and ionic strength was corrected with KCl. The dashed line represents a 200 μM Fe(III) + 100 μM R5P control. The dotted line shows Fe(III) control. One representative of three experiments is shown. AU, absorbance unit.

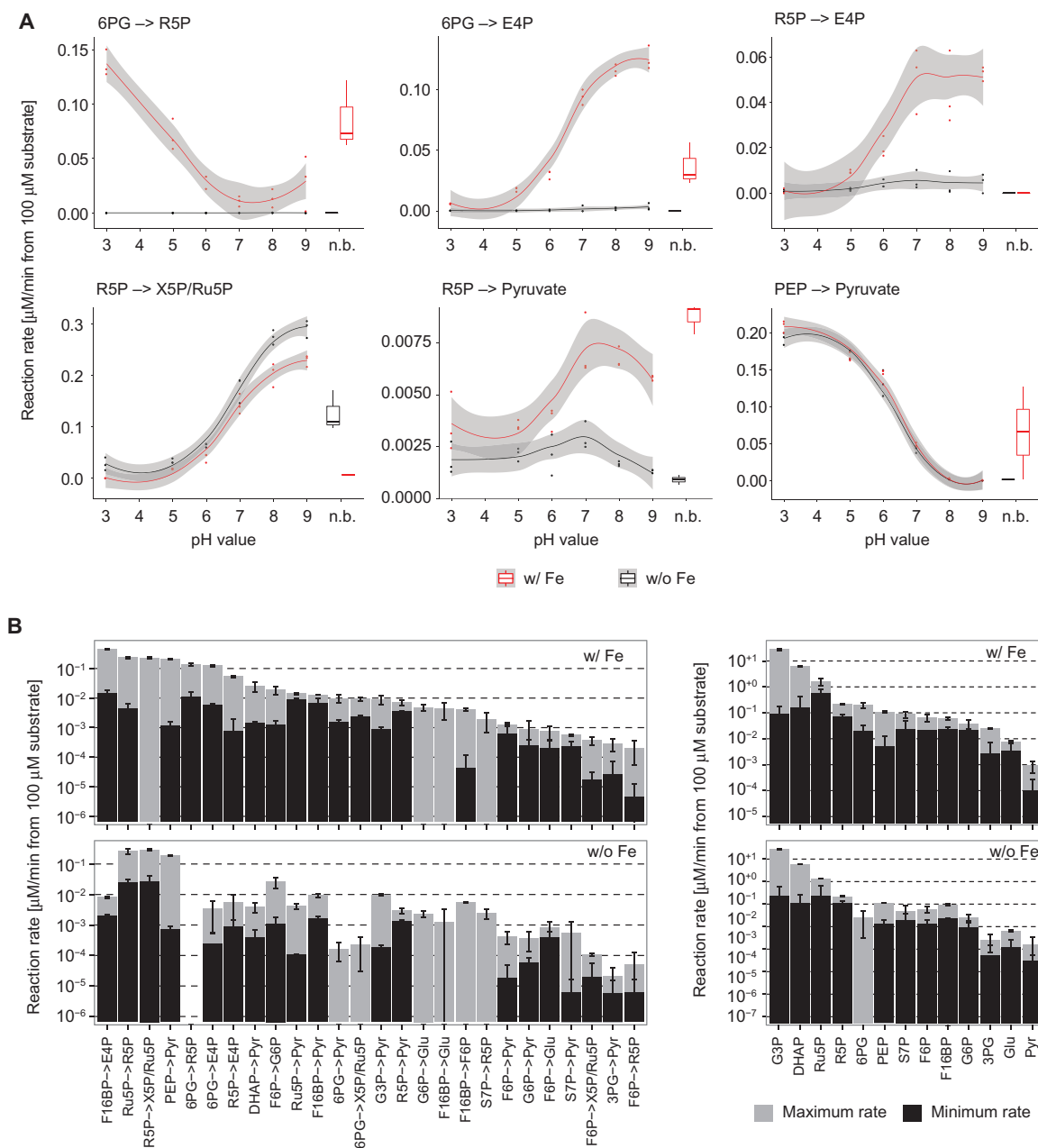


Fig. 3. pH dependency of metabolism-like non-enzymatic sugar phosphate reactivity. (A) Detailed pH dependence profile for non-enzymatic reactions starting from metabolites shown above (6PG, R5P, and PEP). Loess function was used for fitting to the experimental data (shown in dots); gray areas indicate confidence intervals (0.95). Data are presented for Fe(II)-containing (red lines) and iron-free (black lines) anoxic conditions. For most reactions, either a clear acidic or alkaline preference could be observed; that is, 6PG converts into R5P at acidic pH, but at high pH, the reaction yields E4P. Boxplots represent rates measured for the same reactions in a nonbuffered solution (n.b.) in the presence (red) or absence (black) of iron. (B) Absolute maximum rates (gray) and absolute minimum rates (black) for all non-enzymatic reactions observed in the presence of iron (upper panel) and in iron-free anoxic environments (lower panels). Data are illustrated as means \pm SD ($n = 3$). All data and respective pH values are given in tables S6 and S7.

rate decreased less (median change of 1.15-fold) (Fig. 3B, right), demonstrating a parallel increase in the specific formation of glycolytic and PPP intermediates.

Using the LC-SRM spectra from more than 4000 samples, we calculated pH reactivity landscapes by fitting metabolite formation rates to a local polynomial regression model (Loess regression) and normalizing to the highest observed reaction rates (Fig. 4A, left and

right panels). Then, to combine the two-dimensional (2D) data of both Fe(II) and pH dependency, we calculated the integral between the Fe(II) and water pH dependency profiles [Fig. 4B; red, Fe(II); black, water]. This analysis revealed that reactions relevant for the metabolic network are clearly faster in the presence of Fe(II) over most of the pH range (Fig. 4B, all red arrows). This is also reflected in the pH dependency of differential reaction rates ($\Delta R_{[w/Fe(II)] - w/o Fe(II)}$)

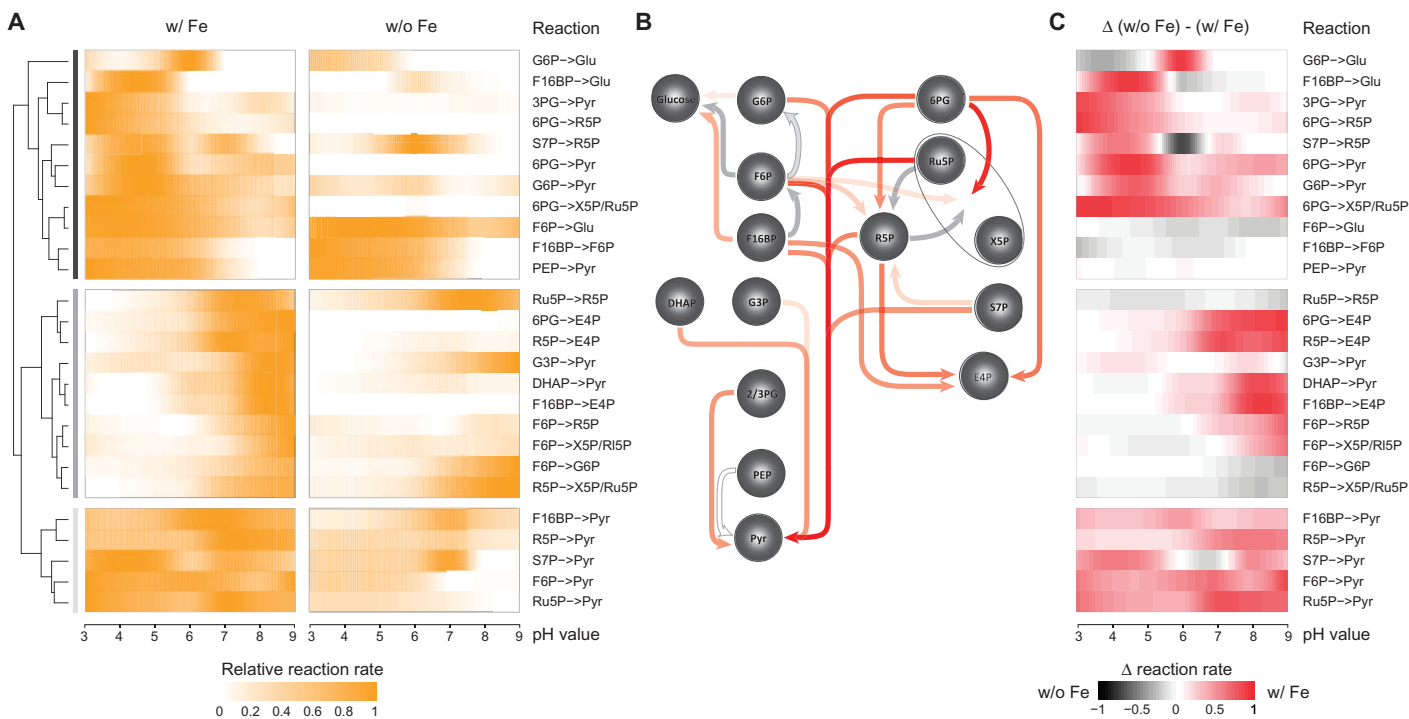


Fig. 4. pH and iron interdependency of non-enzymatic glycolysis and PPP pendants. (A) pH-dependent changes expressed as relative individual reaction rates, calculated by fitting a Loess model to the experimental data and normalizing to the highest rate in iron-containing (left panel) or iron-free (right panel) solutions, as a function of pH. Hierarchical clustering on Fe(II) profiles separated the reactions into three groups: those accelerated under (i) acidic or (ii) alkaline conditions and (iii) reactions with slow overall rate but broad pH range. (B) Iron dependency in a glycolysis- and PPP-like network graph assembled from the non-enzymatic reactions, expressing the values determined over a pH range from 3 to 9. Most reactions are accelerated (red arrows), and a minority is slowed (black arrows) by iron, whereas some are, at stabilized pH, iron-independent (white arrows). (C) Differences in non-enzymatic reactivity between an iron-rich and iron-free anoxic milieu expressed as ΔR . Red indicates higher conversion rates in an iron-rich environment, whereas black shows higher reactivity when no iron is present.

(Fig. 4C): pH ranges with a strong accelerating effect of iron on the reaction rate are colored in red, which is true for a series of reactions under acidic ($n = 9$) and basic ($n = 9$) conditions. The effect of iron on specific reactivity corresponds to the overall rate acceleration (compare Fig. 4A). An analogous analysis for substrate stability/consumption rates revealed that, for most of the reactions, the consumption of a metabolite increases when specific products are formed, confirming increased specificity (fig. S8).

Hierarchical clustering of pH/iron interdependency profiles divided the reactions in three principal groups, which, remarkably, replicate to a certain extent the topology of the cellular metabolic network: (i) The first cluster consists of 11 reactions that preferentially occur in an acidic environment and included the pentose phosphate isomerizations ($6PG \rightarrow X5P/Ru5P$ and $6PG \rightarrow R5P$) and the glycolytic dephosphorylation reactions ($PEP \rightarrow Pyr$, $3PG \rightarrow Pyr$, $F16BP \rightarrow F6P$, and $G6P \rightarrow Glu$). (ii) The second cluster is composed of reactions ($n = 10$) highly accelerated under alkaline conditions and corresponds to the nonoxidative part of the PPP ($Ru5P \rightarrow R5P$, $R5P \rightarrow E4P$, and $F6P \rightarrow R5P$) and six-carbon phosphate isomerization ($F6P \rightarrow G6P$) or a combination of these ($F6P \rightarrow E4P$). (iii) Finally, the last group ($n = 5$) exhibits a broad pH preference profile and converts a sugar phosphate (F16BP, R5P, S7P, F6P, or Ru5P) to Pyr. These represent the multistep reactions with comparably low total rate (Fig. 3B), in which reactions with different pH optima sequentially occur until Pyr is formed, and hence, these resemble glycolysis.

DISCUSSION

The origin of metabolism during the origin of life distinguishes two problems: (i) How did the very first biomolecules form, and where and how did they accumulate to achieve life-compatible concentration? (ii) Upon the origin of life, how have cells learned to establish a metabolic network and to self-synthesize these components? Considerable progress has been made to understand the first problem, for instance, in recent work from Patel and co-workers that proposes a common chemical origin of the life-supporting building blocks from a small set of abiotic precursors driven by UV light and transition metal-accelerated redox cycles (4). Coupled to an Archean environment-constrained reaction space available for these molecules, such systems could have led to self-organization of such a prebiotic chemical system (11, 34, 35).

However, little is known about the other problem, the origin of the metabolic network. Oparin noted that “from a purely chemical standpoint assimilation and dissimilation, the whole of metabolism, is a complicated association of an enormous number of extremely simple and relatively uniform reactions” (36). A century of biochemical research has largely confirmed his assumption; most reactions that participate in metabolism are chemically relatively simple, with repetitive reaction mechanisms, so that enzymes can be classified in solely six categories (37, 38). However, metabolism acquires complexity through the parallel occurrence of many of these simple reactions. There is a long-lasting debate of whether these reactions emerged as the result of evolutionary selection of enzymatic catalysts or whether they are

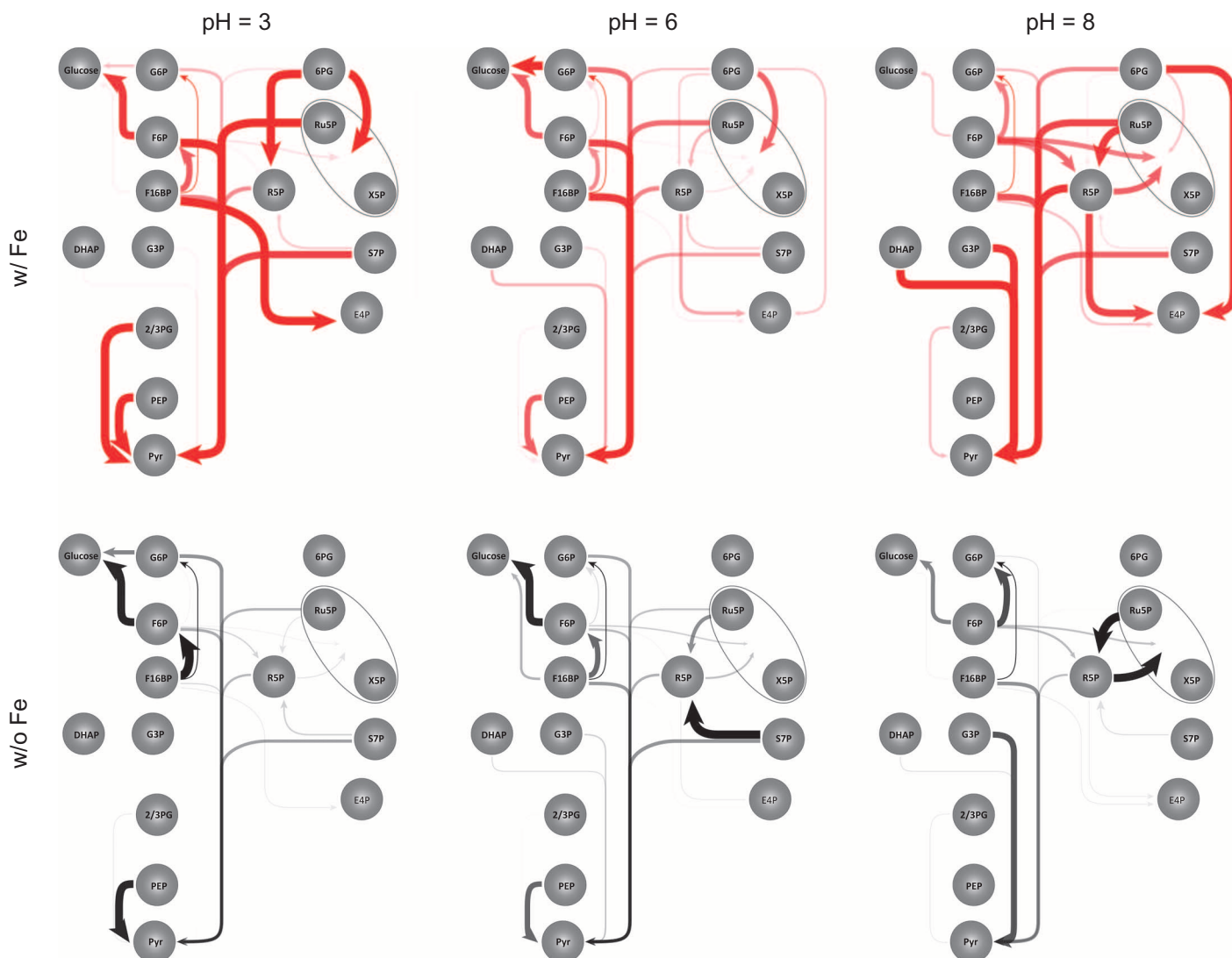


Fig. 5. Conditional activity of a metabolism-like chemical network assembled from non-enzymatic reactions. Observed non-enzymatic reactions were illustrated according to the topology of the Embden-Meyerhof pathway and PPP. Arrow thickness and color intensity indicate the relative acceleration of the reaction at pH 3, 6, and 8 and in the presence (top panel, red) and absence (lower panel, black) of Fe(II). At neutral or slightly acidic pH, multistep reactions representing glycolysis are mostly active, whereas little reactivity in the PPP is observed. At alkaline pH, the PPP and lower glycolysis gain activity. Strongly acidic pH instead favors pentose isomerization and the formation of nonphosphorylated Glu and Pyr.

of environmental-chemical origin (13, 17, 39). Despite the universality of protein-based enzymes in modern metabolic networks, difficulties in explaining the origin of metabolism by genetic selection principles led Morowitz (40), De Duve (41), Wächtershäuser (16), Eschenmoser (42), and others to formulate a conceptual and theoretical framework for a non-enzymatic origin of metabolism. Recently, we could demonstrate the occurrence of non-enzymatic glycolysis and PPP-like reactivity in reconstructed primordial reaction milieus whose salt and metallic compositions oriented on the composition of Archean oceanic sediments and that contained Fe(II), their predominant metal constituent (19). This finding provides experimental evidence for a non-enzymatic origin of metabolic pathways operating within central carbon metabolism.

We found these reactions to be sensitive to the metal constituents. In an early evolutionary context, a metal-dependent reaction network

forms a highly attractive hypothesis that may provide a stepwise scenario for the origin of metabolic enzymes (13). Whereas iron solubility is very limited today due to oxidation to Fe(III) [0.2 to 1.2 nM at pH 7 (43); today's oceans contain less than 0.5 nM iron], reduced Fe(II) is readily water-soluble (26). The Fe(II) concentration of the Archean aquatic environments has suggested around 200 μM , but even higher concentrations of up to 1.2 mM are recently considered (44, 45). Iron was thus abundantly available to first aquatic organisms. If a metabolic pathway started as a series of Fe(II)-dependent reactions, it follows that a simple RNA or peptide molecule with binding affinity for a metal could accelerate all participating reactions in parallel, providing a simple structure that is advantageous to multiple reactions in parallel. Moreover, the anionic groups of RNA or peptide molecules can facilitate Fe(II) binding. In a second step, a metal/RNA or metal/peptide complex would form an ideal template for the selection of more

complex sequences to improve substrate affinity and specificity. In favor of a metal-dependent origin of many metabolic enzymes is that metal ions remain frequently associated with enzyme catalysis; one-third of all enzymes require a metal center for their function (46). Several metal-independent enzymes of higher eukaryotes, for instance, R5P epimerase in the PPP, have metal-dependent counterparts in bacteria and single cellular organisms (47). This implies that, in early organisms, metal catalysis could have been even more widespread and got reduced over the evolutionary time line.

We find metabolism-like, non-enzymatic glycolytic and PPP reactivity dominated by iron; nevertheless, other metal ions such as cobalt, nickel, or molybdenum did also catalyze non-enzymatic sugar phosphate interconversions, although with limited capacity (text S1). The formation of iron-metabolite complexes is dynamic, depending on oxidation state and pH (Figs. 1 and 2) with negatively charged phosphate and carboxyl and, to a smaller extent, also polar hydroxyl groups mediating reactivity. Because of the multitude of possible molecular intermediates, the physicochemical details of Fe-ligand interaction are generally considered complex (48). Our results agree with other previously elaborated examples of iron/carbohydrate chemistry; for instance, the well-studied Fe(III)-citrate interactions involve a variety of mono- and polynuclear complexes whose stable formation depends on their relative concentrations, functional group pK_a , and pH (31). Also, the reactions studied herein show (i) strong acceleration of 10- to 100-fold in the presence of iron, (ii) a similarly sized pH-dependent dynamic range, or (iii) a combination of both effects—which is the case for most of the reactions.

In total, we describe 26 reactions that participate in the network, 17 of which are affected by >10-fold pH in the buffer range of 3 to 9 provided by the phosphate buffer. Also, more extreme pH values exceeding 10 would be accessible in geological environments (49) and could result in an even broader spectrum. However, such extreme pH conditions are of minor relevance for cellular metabolic networks and hence have not been addressed in the present paper. The large consequences are illustrated by a multistep reaction sequence resembling the non-enzymatic PPP. This sequence starts with decarboxylation of 6PG as catalyzed by 6PG dehydrogenase in cells. Fe(II) is a known specific catalyst for decarboxylations of α -keto carboxylic acids (50), a mechanism with potential compatibility with the α -hydroxyl-bearing 6PG. This decarboxylation is followed by subsequent isomerization, yielding analog with PPP, a mixture of the pentose phosphates X5P/Ru5P and R5P. These are then further converted, eventually forming E4P and Pyr. Hence, the final products are the results of multistep rearrangements, including C-C bond breakages and dephosphorylation. In total, this reaction sequence is 30- to 50-fold accelerated by Fe(II) (table S8).

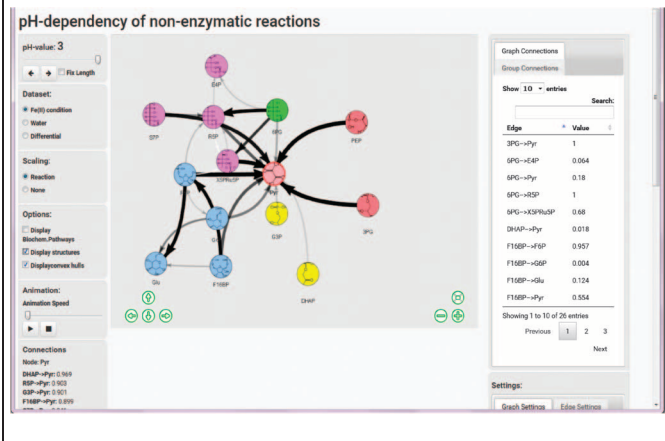
Isomerization reactions among five and six carbon sugars were strongly pH-dependent (R5P→Ru5P/X5P, Ru5P→R5P, F6P→G6P). However, this cannot be generally expected for isomerizations because, for example, non-enzymatic prolyl cis-trans isomerization is not pH-dependent (51). This suggests that, although hydrogen ions are neither consumed nor released in the overall reaction, intermediate steps are pH-sensitive. Consistently, R5P is in a pH-dependent manner found in multiple conformations including ribofuranose and ribopyranose (52). The C1-OH of the pyranoside conformation has been recently described as the preferred site of initial ionization when pH is alkaline ($pK_a = 11.8$) (53), compatible with the non-enzymatic pH optimum at pH >8 observed here (Fig. 4A). An analogous trend is also found

for enzymes that catalyze these reactions in modern cells that operate at an optimum of pH 8 to 8.5 (fig. S7). Also, the retroaldol/aldol mechanism proposed for Ru5P epimerase requires an initial base-catalyzed deprotonation (54), giving credence to initiating a pH-dependent ionization step.

Each pH favors certain reactions while suppressing others. Mapping a network graph that orients along the structure of Embden-Meyerhof pathway and the PPP (Fig. 5 and Box 1) reveals conditional activity within the network that is also observed in modern cells: in Fe(II)-rich acidic conditions, lower glycolysis and Pyr formations dominate; neutral pH (6 to 7) favors glycolysis, whereas PPP reactions are largely inactive; and alkaline pH (>8) activates the oxidative and nonoxidative PPP reactions. In the absence of iron, the network is far less connected and active, but some pH dependency remains (Fig. 5, lower panel). In this respect, the abovementioned interdependence of Fe(II) availability and pH establishes a feedback between pH-dependent activation of specific reactions and the state of the metal catalyst.

In modern cells, cellular pH is a function of growth, metabolic activity, and stressors (55, 56), and enzyme-catalyzed metabolic reactions are dependent on pH (38). Several glycolytic enzymes are strongly pH-dependent, and changes in cytosolic pH can be associated with blockage of lower glycolysis (57) and regulate the activity of large parts of metabolism (58). We find that, at least for some enzymes, the pH optimum overlaps with their respective non-enzymatic reactions (fig. S7). Potentially, pH dependency of modern glycolysis and PPP hence persists since the origins of metabolism. Indeed, a variety of different pH conditions were available to first organisms, from alkaline environments around hydrothermal vents at pH 9 to 10 (59, 60) to oceans locally acidified by high quantities of dissolved CO₂ and Fe(II) oxidation (61, 62). Other pH gradients establish as a consequence of membrane potential differences (8, 63). Also, non-enzymatic reactions affect environmental pH, for example, by releasing CO₂, thereby influencing

Box 1. A web-based application to interactively change pH and the presence of iron in a network assembled from metabolism-like non-enzymatic reactions. To illustrate this for the interested reader, and for educational purposes to teach about reaction networks, we programmed a Java application, where the pH can be altered systematically and the change in network topology is followed graphically in a data-driven interactive figure at <http://1d3.github.io/graph/> (runs best in Google Chrome browser, free and open to use). This plug-in also enables illustration of the Embden-Meyerhof pathway and allows comparison of the structural similarities of the non-enzymatic pathway with enzyme-catalyzed pathway. It also contains an "Animation" button, where the network changes with increasing pH can be visualized in an animated fashion. Individual reaction rate data can be found in table S9.



their own reactivity. Metabolism in the first organisms could thus profit from changes in pH to avoid constitutive activity.

In conclusion, Fe(II) serves as both catalyst and cosubstrate to mediate a pH-dependent, anoxic, non-enzymatic interconversion network among metabolic sugar phosphate metabolites that reflects modern glycolytic pathway and PPP in several aspects. Together with geological records that reveal the prevalence of Fe(II) in aqueous environments of the anoxic prebiotic world, the existence and specificity of these reactions imply that pathways of central carbon metabolism could directly originate from pre-enzymatic metal/sugar phosphate chemistry. We find reactions with the same pH optimum neighbor in an experimentally functional reaction network that shares topological similarity with modern cell's glycolytic pathway and PPP. The coexistence of different pH optima in different parts of the network allows conditional activity, as it does in the modern cell. This implies that changing chemical conditions can, at least in a rudimentary sense, mimic an essential feature of the modern metabolic network, which is to regulate metabolism by the ability to turn metabolic pathways on and off.

MATERIALS AND METHODS

Methods summary

Ferrous ion concentrations have been measured with ferrozine and ferric ion photospectroscopically. NMR experiments were carried out using an AVANCE II+ (Bruker) NMR spectrometer operating at 500.13 MHz for the ^1H frequency, using a 5-mm triple resonance/X-nucleus/inverse detection (TXI) probe. LC-MS/MS was conducted on an Agilent 1290 UPLC coupled to a 6460 Triple Quadrupole mass spectrometer using an ion pairing method as described previously by Keller *et al.* (19). Data were obtained upon manually supervised peak integration and analyzed in R.

Ferrozine assay for measuring ferrous ion concentration

The concentration of free Fe(II) was determined spectrophotometrically by measuring ferrous iron-ferrozine [3-(2-pyridyl)-5,6-bis(4-phenylsulfonic acid)-1,2,4-triazine, Sigma] complex formation by its absorbance at 562 nm (64). Samples were combined with ferrozine in ammonium acetate buffer (final concentrations: 8 and 13 mM, respectively). The absolute concentration of ferrous ions in samples was quantified using an external standard dilution series of FeCl_2 and FeCl_3 .

Spectrophotometric method for measuring ferric ion concentration

Absorption spectra of solutions with 100 μM R5P and 200 μM FeCl_2 in ultraperformance liquid chromatography (UPLC)-grade water (Biosolve Chemicals) under varied conditions were recorded in the range from 190 to 600 nm in 1-nm steps in quartz cuvettes at 20° to 25°C (Amersham Biosciences) [adapted from Silva *et al.* (31)]. The pH was adjusted by addition of either 0.1 M potassium hydroxide or 0.1 M hydrochloric acid to no more than 1% of total volume and measured with a Hamilton MiniTrode pH electrode (Hamilton). Total ion concentrations were adjusted by addition of complementing amounts of 0.1 M KCl. Control experiments were conducted with R5P and FeCl_2 and FeCl_3 alone.

NMR studies of metabolite iron interaction

Samples of 20 mM R5P or 6PG were prepared in deuterated water buffer containing 0.05 mM trimethylsilyl propanoic acid (TSP) as inter-

nal standard and sodium azide with a final substrate concentration of 20 mM. FeCl_2 or FeCl_3 was added at concentrations of 0, 0.2, 1, 1.5, 2, 2.5, 3, 3.5, 4, 6, 10, and 20 mM. Oxygen was removed from the samples by three repeated vacuum/ N_2 gas cycles before the sample tubes were sealed in an anoxic chamber (Coy Laboratory Products). As a control, similar experiments were conducted using triethylamine as substrates in combination with ferrous iron. NMR experiments were carried out using an AVANCE II+ (Bruker) NMR spectrometer operating at 500.13 MHz for the ^1H frequency, using a 5-mm TXI probe. Basic 1D spectra were collected using a solvent suppression pulse sequence based on a 1D version of the nuclear Overhauser effect spectroscopy pulse sequence to saturate the residual ^1H water signal (relaxation delay, 2 s; T_1 increment, 3 μs ; mixing time, 150 ms; solvent presaturation applied during the relaxation time and the mixing time). One hundred twenty-eight transients were collected into 16-K data points over a spectral width of 12 ppm at 298 K.

Longitudinal relaxation times were measured using the inversion recovery pulse sequence, 180- τ -90, with pulse spacing τ having the following values: 0.01, 0.02, 0.03, 0.05, 0.1, 0.25, 0.5, 0.75, 1, 1.5, 2, 4, 8, 15, 20, and 25 s. The pulse repetition time was set at 20 s. Eight transients were collected into 16-K data points over a spectral width of 20 ppm at 298 K.

One-dimensional NMR spectra were processed using TopSpin version 3.2 (Bruker). Free induction decays were Fourier-transformed following multiplication by a line broadening of 1 Hz and referenced to TSP at 0.0 ppm. Spectra were automatically phase- and baseline-corrected. For the relaxation times, data were analyzed using the T_1/T_2 relaxation module present in TopSpin. After Fourier-transforming, phasing, and baseline-correcting the spectra, peaks corresponding to the different protons in the molecule were integrated for each of the 16 points measured. The resulting curves were fitted using the Levenberg-Marquardt algorithm according to the equation

$$I(t) = I_0 + P * \exp\left(-\frac{t}{T_1}\right)$$

where I_0 is the intensity of the magnetization at time 0, T_1 is the longitudinal relaxation time, and P is a parameter that takes into account the 90° radio-frequency pulse imperfection (fig. S5).

Interconversion time course experiments

Metabolite standards were obtained from Sigma-Aldrich at the highest purity available: Glu (product no. 16325), G6P (G7879), F6P (F3627), F16BP (F6803), glyceraldehyde 3-phosphate (G5251), dihydroxyacetone phosphate (D7137), 3PG (P8877), PEP (P7127), Pyr (P2256), 6-phosphogluconic acid (P7877), R5P (82875), Ru5P (83899), and S7P (78832). All water (Biosolve Chemicals, catalog no. 23214102) used was of UPLC-MS grade.

Incubations of individual metabolites were performed in sealed high-performance liquid chromatography (HPLC) vials (5182-0717 and 5182-0716, Agilent Technologies) heated to 70°C in a water bath. For all samples other than Pyr and Glu, sampling was performed after 0, 10, 30, 60, 120, and 300 min by rapid cooling on ice. For Pyr and Glu, sampling was performed at 0, 24, and 168 hours because of their stability under the reaction conditions. Initial metabolite concentrations were 100 μM . The effect of pH on metabolite reactivity was investigated by buffering at pH points 3, 5, 6, 7, 8, and 9 with 5 mM sodium phosphate. pH values were initially measured, although during incubations, the

pH was controlled via the buffer capacity of the respective buffer. Iron was added as 200 μM iron(II) chloride (Sigma-Aldrich, 372870), and a separate set of reactions was performed by adding water instead. Buffer and sugar phosphate mixtures were prepared fresh. Vials were sealed in an anoxic chamber (Coy Laboratory Products), with oxygen removed by three repeated vacuum/ N_2 gas cycles. Following incubation, the reactions were stopped on ice, and samples were transferred to 384-well plates (Greiner Bio-One, 781186) under normoxic conditions and stored at -80°C until thawed for HPLC-MS/MS measurement.

LC-SRM and data analysis

Sugar phosphates were quantified as previously described by Keller *et al.* (19) using an online coupled HPLC system (Agilent 1290) and triple-quadrupole mass analyzer (Agilent 6460) operating in SRM mode (see MS Tables S1 to S4 for details). Separation was achieved on a C8 column [Zorbax SB-C8 Rapid Resolution HD, 2.1×100 mm, $1.8 \mu\text{m}$ (Agilent); column temperature, 30°C] with an acetonitrile/water gradient (Greyhound Chemicals) over a 7.5-min cycle per sample. Running buffers contained octylammonium acetate (750 mg/liter) prepared from octylamine (Sigma-Aldrich, O5802), as described by Wamelink *et al.* (30). All above experiments were performed in triplicate.

Data presented herein are the products of the analysis of 3024 LC-SRM runs on samples, plus more than 1000 runs used for external standards, blanks, and controls. MS/MS data were analyzed with MassHunter Workstation (Agilent) using QQQ Quantitative Analysis Software package. All automated peak integrations were manually curated, and manual supervision ensured consistency with regularly measured quality control standards. Absolute concentrations were determined by comparison to repeatedly measured external standard dilution series. Analysis and fitting of reaction rates were performed in R (R Core Team, www.R-project.org).

Study design

The sample size in this systematic study was selected according to the requirements for an optimal coverage of the possible reaction space, constrained by time, quality, and methodological requirements of the mass spectrometry measurements. In total, more than 4000 samples were measured (three-fourth samples and one-fourth controls and standards). The samples were prepared in at least three individual replicates. Rarely occurring outliers were not excluded from the data set because functions chosen for fitting reaction rate data were robust against single inaccurate values. Time points for time series measurements were selected according to our previous experiences with comparable experiments (19), allowing to quantify fast and relatively slow non-enzymatic interconversions within the same experiment.

SUPPLEMENTARY MATERIALS

Supplementary material for this article is available at <http://advances.sciencemag.org/cgi/content/full/2/1/e1501235/DC1>

MS Table S1. MS/MS parameters.

MS Table S2. UPLC/HPLC parameters.

MS Table S3. HPLC gradient.

MS Table S4. Q1/Q3 (SRM) transitions and parameters.

Fig. S1. ^1H NMR spectra of R5P and Fe(II) mixtures.

Fig. S2. ^1H NMR spectra of R5P and Fe(III) mixtures.

Fig. S3. ^1H NMR spectra of 6PG and Fe(II) mixtures.

Fig. S4. ^1H NMR spectra of triethylamine and Fe(III) mixtures.

Fig. S5. T_1 NMR experiment curve-fitting examples [example of 6PG and Fe(II)].

Fig. S6. Ferrozine results: Fe(II)/Fe(III) in dependence of pH.

Fig. S7. Enzymatic pH dependency of ribose-phosphate isomerase and comparison to its non-enzymatic counterpart (R5P \rightarrow X5P/Ru5P).

Fig. S8. pH and iron dependency on non-enzymatic substrate consumption rates.

Fig. S9. Comparison of Fe(II)- and pH-facilitated non-enzymatic reactivity with the reaction network structure facilitated by a mixture of prebiotically plausible ocean metals [Keller *et al.* (19)].

Table S1. T_1 relaxation time of R5P and Fe(II) mixtures.

Table S2. T_1 relaxation time of R5P and Fe(III) mixtures.

Table S3. T_1 relaxation time of 6PG and Fe(II) mixtures.

Table S4. T_1 relaxation time of triethylamine and Fe(II) mixtures.

Table S5. Integrated NMR peak areas for all individual iron-sugar phosphate interaction NMR experiments.

Table S6. Maximum and minimum reaction rates of non-enzymatic interconversions between sugar phosphates in the presence of Fe(II).

Table S7. Maximum and minimum reaction rates of non-enzymatic interconversions between sugar phosphates in the absence of Fe(II).

Table S8. Relative acceleration of non-enzymatic interconversions between sugar phosphates by pH and iron availability and possible mechanistic rationale.

Table S9. Individual reaction rates of non-enzymatic interconversions between sugar phosphates in the presence and absence of Fe(II).

Text S1. Comparison of the reactions found here and in previous work [Keller *et al.* (19)] in which sediment-like complex metal mixtures were studied.

References (65–69)

REFERENCES AND NOTES

- B. Herschy, A. Whicher, E. Camprubi, C. Watson, L. Dartnell, J. Ward, J. R. G. Evans, N. Lane, An origin-of-life reactor to simulate alkaline hydrothermal vents. *J. Mol. Evol.* **79**, 213–227 (2014).
- D. Ritson, J. D. Sutherland, Prebiotic synthesis of simple sugars by photoredox systems chemistry. *Nat. Chem.* **4**, 895–899 (2012).
- C. Huber, G. Wächtershäuser, α -Hydroxy and α -amino acids under possible Hadean, volcanic origin-of-life conditions. *Science* **314**, 630–632 (2006).
- B. H. Patel, C. Percivalle, D. J. Ritson, C. D. Duffy, J. D. Sutherland, Common origins of RNA, protein and lipid precursors in a cyanosulfidic protometabolism. *Nat. Chem.* **7**, 301–307 (2015).
- M. W. Powner, B. Gerland, J. D. Sutherland, Synthesis of activated pyrimidine ribonucleotides in prebiotically plausible conditions. *Nature* **459**, 239–242 (2009).
- M. A. Pasek, J. P. Harnmeijer, R. Buick, M. Gull, Z. Atlas, Evidence for reactive reduced phosphorus species in the early Archean ocean. *Proc. Natl. Acad. Sci. U.S.A.* **110**, 10089–10094 (2013).
- W. Martin, M. J. Russell, On the origin of biochemistry at an alkaline hydrothermal vent. *Philos. Trans. R. Soc. Lond. B Biol. Sci.* **362**, 1887–1925 (2007).
- N. Lane, W. F. Martin, The origin of membrane bioenergetics. *Cell* **151**, 1406–1416 (2012).
- N. H. Horowitz, On the evolution of biochemical syntheses. *Proc. Natl. Acad. Sci. U.S.A.* **31**, 153–157 (1945).
- H. Hartman, Speculations on the origin and evolution of metabolism. *J. Mol. Evol.* **4**, 359–370 (1975).
- E. Smith, H. J. Morowitz, Universality in intermediary metabolism. *Proc. Natl. Acad. Sci. U.S.A.* **101**, 13168–13173 (2004).
- C. de Duve, Chemistry and selection. *Chem. Biodivers.* **4**, 574–583 (2007).
- M. Ralser, The RNA world and the origin of metabolic enzymes. *Biochem. Soc. Trans.* **42**, 985–988 (2014).
- H. J. Morowitz, J. D. Kostelnik, J. Yang, G. D. Cody, The origin of intermediary metabolism. *Proc. Natl. Acad. Sci. U.S.A.* **97**, 7704–7708 (2000).
- G. Wächtershäuser, Before enzymes and templates: Theory of surface metabolism. *Microbiol. Rev.* **52**, 452–484 (1988).
- G. Wächtershäuser, Evolution of the first metabolic cycles. *Proc. Natl. Acad. Sci. U.S.A.* **87**, 200–204 (1990).
- L. E. Orgel, Prebiotic chemistry and the origin of the RNA world. *Crit. Rev. Biochem. Mol. Biol.* **39**, 99–123 (2004).
- J. P. Amend, D. E. LaRowe, T. M. McCollom, E. L. Shock, The energetics of organic synthesis inside and outside the cell. *Philos. Trans. R. Soc. Lond. B Biol. Sci.* **368**, 20120255 (2013).
- M. A. Keller, A. V. Turchyn, M. Ralser, Non-enzymatic glycolysis and pentose phosphate pathway-like reactions in a plausible Archean ocean. *Mol. Syst. Biol.* **10**, 725 (2014).
- A. Bar-Even, E. Noor, Y. Savir, W. Liebermeister, D. Davidi, D. S. Tawfik, R. Milo, The moderately efficient enzyme: Evolutionary and physicochemical trends shaping enzyme parameters. *Biochemistry* **50**, 4402–4410 (2011).
- J. Peretó, Out of fuzzy chemistry: From prebiotic chemistry to metabolic networks. *Chem. Soc. Rev.* **41**, 5394–5403 (2012).

22. L. A. Fothergill-Gillmore, P. A. M. Michels, Evolution of glycolysis. *Prog. Biophys. Mol. Biol.* **59**, 105–235 (1993).
23. C. Schnarrenberger, W. Martin, Evolution of the enzymes of the citric acid cycle and the glyoxylate cycle of higher plants. A case study of endosymbiotic gene transfer. *Eur. J. Biochem.* **269**, 868–883 (2002).
24. A. Stincone, A. Prigione, T. Cramer, M. M. C. Wamelink, K. Campbell, E. Cheung, V. Olin-Sandoval, N.-M. Grüning, A. Krüger, M. T. Alam, M. A. Keller, M. Breitenbach, K. M. Brindle, J. D. Rabinowitz, M. Ralse, The return of metabolism: Biochemistry and physiology of the pentose phosphate pathway. *Biol. Rev. Camb. Philos. Soc.* **90**, 927–963 (2015).
25. D. E. Canfield, The Archean sulfur cycle and the early history of atmospheric oxygen. *Science* **288**, 658–661 (2000).
26. O. J. Rouxel, A. Bekker, K. J. Edwards, Iron isotope constraints on the Archean and Paleoproterozoic ocean redox state. *Science* **307**, 1088–1091 (2005).
27. I. Bertini, C. Luchinat, *NMR of Paramagnetic Molecules in Biological Systems* (Benjamin/Cummings Publishing Company, Menlo Park, CA, 1986).
28. I. Solomon, Relaxation processes in a system of two spins. *Phys. Rev.* **99**, 559–565 (1955).
29. N. Bloembergen, E. M. Purcell, R. V. Pound, Relaxation effects in nuclear magnetic resonance absorption. *Phys. Rev.* **73**, 679–712 (1948).
30. M. M. C. Wamelink, E. A. Struys, J. H. J. Huck, B. Roos, M. S. van der Knaap, C. Jakobs, N. M. Verhoeven, Quantification of sugar phosphate intermediates of the pentose phosphate pathway by LC-MS/MS: Application to two new inherited defects of metabolism. *J. Chromatogr. B Analyt. Technol. Biomed. Life Sci.* **823**, 18–25 (2005).
31. A. M. N. Silva, X. Kong, M. C. Parkin, R. Cammack, R. C. Hider, Iron(III) citrate speciation in aqueous solution. *Dalton Trans.* 8616–8625 (2009).
32. P. Van Cappellen, E. D. Ingall, Redox stabilization of the atmosphere and oceans by phosphorus-limited marine productivity. *Science* **271**, 493–496 (1996).
33. J. Pierce, A. S. Serianni, R. Barker, Anomerization of furanose sugars and sugar phosphates. *J. Am. Chem. Soc.* **107**, 2448–2456 (1985).
34. A. Pross, How can a chemical system act purposefully? Bridging between life and non-life. *J. Phys. Org. Chem.* **21**, 724–730 (2008).
35. A. Eschenmoser, Etiology of potentially primordial biomolecular structures: From vitamin B₁₂ to the nucleic acids and an inquiry into the chemistry of life's origin: A retrospective. *Angew. Chem. Int. Ed. Engl.* **50**, 12412–12472 (2011).
36. A. I. Oparin, *The Origin of Life on the Earth* (Oliver and Boyd, London, 1957).
37. A. J. Barrett; Nomenclature Committee of the International Union of Biochemistry and Molecular Biology (NC-IUBMB), Enzyme nomenclature. Recommendations 1992. Supplement 2: Corrections and additions (1994). *Eur. J. Biochem.* **232**, 1–6 (1995).
38. M. A. Keller, G. Piedrafita, M. Ralsler, The widespread role of non-enzymatic reactions in cellular metabolism. *Curr. Opin. Biotechnol.* **34**, 153–161 (2015).
39. A. Lazcano, S. L. Miller, On the origin of metabolic pathways. *J. Mol. Evol.* **49**, 424–431 (1999).
40. H. J. Morowitz, *Beginnings of Cellular Life: Metabolism Recapitulates Biogenesis* (Yale Univ. Press, New Haven, CT, 1992).
41. C. De Duve, *Singularities: Landmarks on the Pathways of Life* (Cambridge Univ. Press, New York, 2005).
42. A. Eschenmoser, The search for the chemistry of life's origin. *Tetrahedron* **63**, 12821–12844 (2007).
43. F. J. Millero, Solubility of Fe(III) in seawater. *Earth Planet. Sci. Lett.* **154**, 323–329 (1998).
44. A. D. Anbar, Oceans. Elements and evolution. *Science* **322**, 1481–1483 (2008).
45. V. Busigny, N. J. Planavsky, D. Jézéquel, S. Crowe, P. Louvat, J. Moureau, E. Viollier, T. W. Lyons, Iron isotopes in an Archean ocean analogue. *Geochim. Cosmochim. Acta* **133**, 443–462 (2014).
46. R. H. Holm, P. Kennepohl, E. I. Solomon, Structural and functional aspects of metal sites in biology. *Chem. Rev.* **96**, 2239–2314 (1996).
47. J. M. Sobota, J. A. Imlay, Iron enzyme ribulose-5-phosphate 3-epimerase in *Escherichia coli* is rapidly damaged by hydrogen peroxide but can be protected by manganese. *Proc. Natl. Acad. Sci. U.S.A.* **108**, 5402–5407 (2011).
48. J. L. Pierre, I. Gautier-Luneau, Iron and citric acid: A fuzzy chemistry of ubiquitous biological relevance. *Biometals* **13**, 91–96 (2000).
49. N. H. Sleep, K. Zahnle, Carbon dioxide cycling and implications for climate on ancient Earth. *J. Geophys. Res.* **106**, 1373–1399 (2001).
50. B. Siegel, J. Lanphear, Iron-catalyzed oxidative decarboxylation of benzoylformic acid. *J. Am. Chem. Soc.* **101**, 2221–2222 (1979).
51. R. L. Stein, Mechanism of enzymatic and nonenzymatic prolyl cis-trans isomerization. *Adv. Protein Chem.* **44**, 1–24 (1993).
52. A. F. Amaral, M. M. Marques, J. A. L. da Silva, J. J. R. Fraústo da Silva, Interactions of D-ribose with polyatomic anions, and alkaline and alkaline-earth cations: Possible clues to environmental synthesis conditions in the pre-RNA world. *New J. Chem.* **32**, 2043–2049 (2008).
53. S. Sudarsan, S. Dethlefsen, L. M. Blank, M. Siemann-Herzberg, A. Schmid, The functional structure of central carbon metabolism in *Pseudomonas putida* KT2440. *Appl. Environ. Microbiol.* **80**, 5292–5303 (2014).
54. J. Samuel, M. E. Tanner, Mechanistic aspects of enzymatic carbohydrate epimerization. *Nat. Prod. Rep.* **19**, 261–277 (2002).
55. M. Valli, M. Sauer, P. Branduardi, N. Borth, D. Porro, D. Mattanovich, Intracellular pH distribution in *Saccharomyces cerevisiae* cell populations, analyzed by flow cytometry. *Appl. Environ. Microbiol.* **71**, 1515–1521 (2005).
56. P. Cimprich, J. Slavík, A. Kotyk, Distribution of individual cytoplasmic pH values in a population of the yeast *Saccharomyces cerevisiae*. *FEMS Microbiol. Lett.* **130**, 245–251 (1995).
57. J. H. van Heerden, M. T. Wortel, F. J. Bruggeman, J. J. Heijnen, Y. J. Bollen, R. Planqué, J. Hulshof, T. G. O'Toole, S. A. Wahl, B. Teusink, Lost in transition: Start-up of glycolysis yields sub-populations of nongrowing cells. *Science* **343**, 1245114 (2014).
58. K. Sakano, Metabolic regulation of pH in plant cells: Role of cytoplasmic pH in defense reaction and secondary metabolism. *Int. Rev. Cytol.* **206**, 1–44 (2001).
59. D. S. Kelley, J. A. Karson, D. K. Blackman, G. L. Früh-Green, D. A. Butterfield, M. D. Lilley, E. J. Olson, M. O. Schrenk, K. K. Roe, G. T. Lebon, P. Rivizzigno; AT3-60 Shipboard Party, An off-axis hydrothermal vent field near the Mid-Atlantic Ridge at 30 degrees N. *Nature* **412**, 145–149 (2001).
60. D. S. Kelley, J. A. Karson, G. L. Früh-Green, D. R. Yoerger, T. M. Shank, D. A. Butterfield, J. M. Hayes, M. O. Schrenk, E. J. Olson, G. Proskurowski, M. Jakuba, A. Bradley, B. Larson, K. Ludwig, D. Glickson, K. Buckman, A. S. Bradley, W. J. Brazelton, K. Roe, M. J. Elend, A. Delacour, S. M. Bernasconi, M. D. Lilley, J. A. Baross, R. E. Summons, S. P. Sylva, A serpentinite-hosted ecosystem: The lost city hydrothermal field. *Science* **307**, 1428–1434 (2005).
61. G. MacLeod, C. McKeown, A. J. Hall, M. J. Russell, Hydrothermal and oceanic pH conditions of possible relevance to the origin of life. *Orig. Life Evol. Biosph.* **24**, 19–41 (1994).
62. M. J. Russell, A. J. Hall, The emergence of life from iron monosulphide bubbles at a submarine hydrothermal redox and pH front. *J. Geol. Soc. London.* **154**, 377–402 (1997).
63. V. Sojo, A. Pomiankowski, N. Lane, A bioenergetic basis for membrane divergence in Archaea and bacteria. *PLOS Biol.* **12**, e1001926 (2014).
64. L. L. Stookey, Ferrozine—A new spectrophotometric reagent for iron. *Anal. Chem.* **42**, 779–781 (1970).
65. A. L. Stern, E. Burgos, L. Salmon, J. J. Cazzulo, Ribose 5-phosphate isomerase type B from *Trypanosoma cruzi*: Kinetic properties and site-directed mutagenesis reveal information about the reaction mechanism. *Biochem. J.* **401**, 279–285 (2007).
66. C.-S. Park, S.-J. Yeom, Y.-R. Lim, Y.-S. Kim, D.-K. Oh, Substrate specificity of a recombinant ribose-5-phosphate isomerase from *Streptococcus pneumoniae* and its application in the production of L-lyxose and L-tagatose. *World J. Microbiol. Biotechnol.* **27**, 743–750 (2010).
67. S.-J. Yeom, E.-S. Seo, Y.-S. Kim, D.-K. Oh, Increased D-allose production by the R132E mutant of ribose-5-phosphate isomerase from *Clostridium thermocellum*. *Appl. Microbiol. Biotechnol.* **89**, 1859–1866 (2011).
68. C. L. Skrudrud, I. M. Gordon, S. Dorwin, X.-H. Yuan, G. Johansson, L. E. Anderson, Purification and characterization of pea chloroplastic phosphoriboisomerase. *Plant Physiol.* **97**, 730–735 (1991).
69. G. F. Domagk, K. M. Doering, R. Chilla, Purification and properties of ribose-phosphate isomerase from *Candida utilis*. *Eur. J. Biochem.* **38**, 259–264 (1973).

Acknowledgments: We thank our laboratory members for invaluable critical discussions, N. M. Grüning and E. Calvani for help in proofreading of the manuscript, and B. Fuisz for generating the data-driven Java document. **Funding:** We acknowledge funding from the Isaac Newton Trust (RG 68998 to M.R.), the Wellcome Trust (RG 093735/Z/10/Z to M.R.), the Royal Society (RG60279 to A.V.T.), and the European Research Council (starting grant 260809 to M.R. and starting grant 307582 to A.V.T.). M.A.K. is supported by an Erwin Schrödinger postdoctoral fellowship [J 3341; Austrian Science Fund (FWF), Austria]. M.R. is a Wellcome Trust Research Career Development and Wellcome-Beit Prize Fellow. **Author contributions:** M.A.K. and M.R. conceived the idea and designed the experiments. M.A.K., A.Z., and C.C. performed the experiment and analyzed the data. C.C. and J.L.G. supervised the NMR experiments. A.V.T. and J.L.G. provided experimental and scientific advice. M.A.K. and M.R. wrote the initial draft of the manuscript. All authors contributed to the finalization of the paper. **Competing interests:** The authors declare that they have no competing interests. **Data and materials availability:** All data needed to evaluate the conclusions in the paper are present in the paper and/or the Supplementary Materials. Additional data related to this paper may be requested from the authors. Requests for data and materials should be addressed to M.A.K. (mk747@cam.ac.uk) and M.R. (mr559@cam.ac.uk).

Submitted 7 September 2015

Accepted 18 November 2015

Published 15 January 2016

10.1126/sciadv.1501235

Citation: M. A. Keller, A. Zylstra, C. Castro, A. V. Turchyn, J. L. Griffin, M. Ralsler, Conditional iron and pH-dependent activity of a non-enzymatic glycolysis and pentose phosphate pathway. *Sci. Adv.* **2**, e1501235 (2016).